Jpn. J. Appl. Phys. Vol. 39 (2000) pp. 2619–2623
Part 1, No. 5A, May 2000

Two-Dimensional Photonic Crystal Waveguides with 60° Bends in a Thin Slab Structure

Naoyuki FUKAYA, Daisuke OHSAKI and Toshihiko BABA
Yokohama National University, Faculty of Engineering, Division of Electrical and Computer Engineering, 79-5 Tokiwadai, Hodogaya-ku, Yokohama 240-8501, Japan

(Received Octover 22, 1999; accepted for publication February 23, 2000)

We experimentally investigated the light propagation characteristics of two-dimensional photonic crystal waveguides, for the first time. The difficulty of fabricating photonic crystals with airholes was reduced by employing a thin slab structure with a GaInAsP high refractive index core, and by employing air and SiO_2 low index claddings. The light propagation through channels composed of a series of defects in the photonic crystal was observed in the wavelength range 1.51–1.55 μm. Smooth propagation was maintained even beyond 60° channel bends. The wavelength and polarization dependence of propagation characteristics as well as the peculiar scattering of light to space were explained by the photonic band theory.

KEYWORDS: photonic crystal, waveguide, semiconductor, GaInAsP, lightwave circuit

1. Introduction

Photonic crystals[1–7] are artificial periodic structures with a period of the order of the optical wavelength. Important properties of photonic crystals are the photonic band gap (PBG) and doping. The former is the wavelength range at which transmission and emission of light is completely inhibited. The latter is the introduction of irregular elements to a uniform crystal. This doping causes the strong resonance and localization of light. The photonic crystal waveguide is a significant application, which uses these properties.[8,9]

In conventional total-reflection-type waveguides, the guided light easily suffers radiation loss at steep bends due to the weak optical confinement. Thus, the bend loss restricts the flexibility of the optical wiring pattern in photonic circuits. This makes photonic circuits so large as to be of the cm^2 order, and restricts the multifunctionality. Photonic crystal waveguides have the potential for eliminating this restriction. They allow low-loss steep bends owing to the strong optical confinement of photonic crystal claddings.[10] So far, there has been some reported experimental demonstrations on such waveguides with large crystals operating at microwave frequencies.[11,12] The light transmission through defect apertures in a three-dimensional (3-D) photonic crystal has also been observed.[13] However, there are no reports on the clear observation of light propagation. This is mainly due to the technical challenge of making submicron fine and deep structures of photonic crystals.

In this study, we employed a two-dimensional (2-D) photonic crystal composed of a thin slab structure with a high index core and low index claddings to solve this problem. It is similar to the so-called *photonic crystal disks* or *photonic crystal slabs*. However, compared with photonic crystal disks having a membrane structure, the employed structure was mechanically stable even against the cleavage of the wafer. This facilitated the incidence of light into the waveguide. As a result, we successfully observed light propagation through the waveguide, for the first time. In addition, we observed the wavelength and polarization dependence, which qualitatively agreed with the photonic band theory.

2. Design

Figure 1 shows the schematic of a waveguide fabricated in this study. The slab core was an epitaxially grown GaInAsP film. The lower cladding was a SiO_2 layer and the upper cladding was air. Such media with a high refractive index contrast allows the strong optical confinement in the vertical direction. Waveguide channels were composed of defects in the photonic crystal with airholes,[14] i.e., a corrugated semiconductor stripe of $\sim$0.7 μm in width. We prepared straight parts and 60° bends in a waveguide pattern, as shown in Fig. 2. The designed diameter of holes and pitch between them are 0.5 μm and 0.6 μm, respectively. Figure 3 shows 2-D photonic band diagrams for this structure, assuming the infinite height of the structure and an equivalent refractive index n_{eq} of the guided mode in the slab. Assuming a core index of 3.35, a lower cladding index of 1.45, an upper cladding index of 1.0 and a core thickness of 0.35 μm at a wavelength $\lambda = 1.55\,\mu$m, which corresponds to the experiment described in the next section, we calculated $n_{eq} = 2.97$ for the transverse electric (TE) polarization and $n_{eq} = 2.63$ for the transverse magnetic (TM) polarization. Bands were obtained independently for the TE and TM polarizations. The airhole photonic crystal exhibits the overlap of PBGs for these two polarizations, known as the so-called full 2-D PBG. However, PBGs are separated for the model of Fig. 2. It is seen in Fig. 3 that the PBG for the TE polarization lies at $\lambda = 1.41$–$2.02\,\mu$m for the pitch a shown in Fig. 2. The PBG for the TM polar-

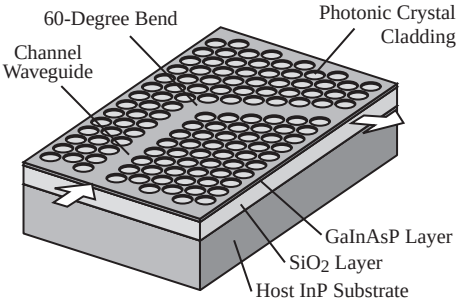

Fig. 1. Schematic of photonic crystal waveguide having a thin slab structure with straight or bent channels and airhole photonic crystal claddings.

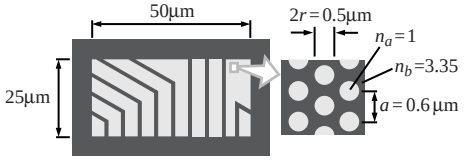

Fig. 2. Designed pattern of photonic crystal waveguide.

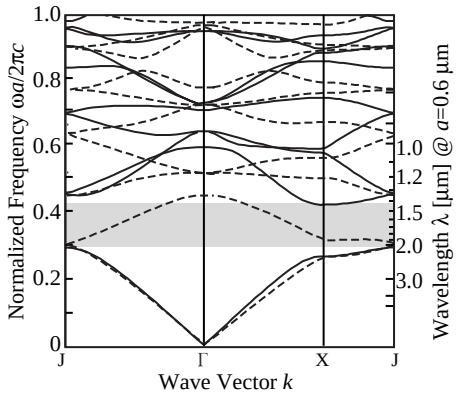

Fig. 3. Photonic band diagram for model of Fig. 2. Solid and dotted curves indicate TE and TM polarizations, respectively.

ization lies at $\lambda = 1.2953$–$1.2965\,\mu$m and is much narrower than the TE PBG. Thus, we expected the propagation of TE polarized light in the waveguide.

3. Fabrication

We prepared an InP wafer with an undoped GaInAsP film of $0.35\,\mu$m thickness and $1.28\,\mu$m electronic bandgap wavelength, which was epitaxially grown by metalorganic vapor phase epitaxy. We fabricated the photonic crystal into the epitaxial film by standard electron beam (EB) lithography with a positive resist ZEP-520 (Nippon Zeon Co., Ltd.) and an electron cyclotron resonance (ECR) plasma etching with a methane-based gaseous source. Figure 4 shows scanning electron micrographs (SEM) of the fabricated photonic crystal. The diameter of holes, except for those beside channels, was $0.45 \pm 0.05\,\mu$m. The diameter of holes beside channels was $0.3 \pm 0.1\,\mu$m. This difference was caused by the nonuniform EB exposure. It can be rectified by the modulated exposure to these holes.[15] The fine structure seen in Fig. 4 was difficult to fabricate into normal waveguides composed of semiconductor layers of $>1.5\,\mu$m total thickness, since a high aspect ratio of over 15 was required for semiconductor walls between holes. This difficulty was drastically reduced by employing the thin slab structure.

We additionally prepared a host InP wafer coated with an SiO_2 layer of $3\,\mu$m thickness by using an RF sputtering method. We bonded these wafers face-to-face using an adhesive World Rock No. 863LNS (Kyoritsu Chemical Inc.). Then, we removed the epitaxial InP substrate by selective wet etching using $HCl : H_2O = 4 : 1$ solution. Figure 5 shows the top view after the bonding process. The photonic crystal pattern was reversed by the bonding process. We also found that holes beside channels were not pierced by the ECR etching due to their small diameters and tilt of etched sidewalls of typically 75° against the substrate plane. Therefore, the width of channels as seen from this side was $\sim 1.6\,\mu$m. In addition, we found some cracks in the GaInAsP film, which were formed during the curing process of the adhesive. Finally, we cleaved the wafer into pieces. We observed the cleaved facet of one piece under an optical microscope, and confirmed that the thickness of the adhesive was less than $0.2\,\mu$m.

In this study, we used the GaInAsP film and adhesive for bonding for our convenience. A direct-transition-type semiconductor, such as GaInAsP, has the potential for various applications to active devices. For waveguides and passive devices, however, they are not necessarily required. One can fabricate a similar structure by using, for example, the direct bonding method of various semiconductors and dielectric materials, such as $Si/SiO_2/Si$ structures by the chemical vapor deposition or by the SOI technique or selective oxidation of an AlAs layer sandwiched by GaAs layers.

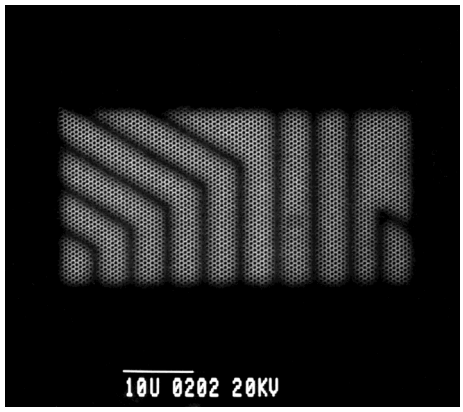

(a)

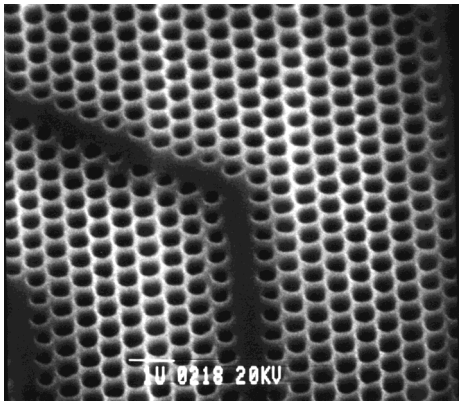

(b)

Fig. 4. Scanning electron micrographs of fabricated photonic crystal. (a) top view of total waveguide pattern and (b) magnified top view of channel and photonic crystal claddings.

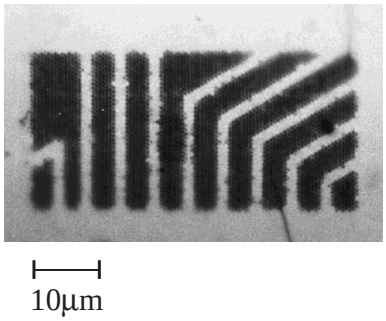

Fig. 5. Top view of waveguide pattern after bonding process.

4. Observation of Light Propagation

Figure 6 shows the schematic of the measurement setup. In the observation of light propagation, a tunable laser TSL-210 (Santec Inc., $\lambda = 1.47$–$1.60\,\mu$m) was used as a light source. We selected TE or TM polarization by inserting a combina-

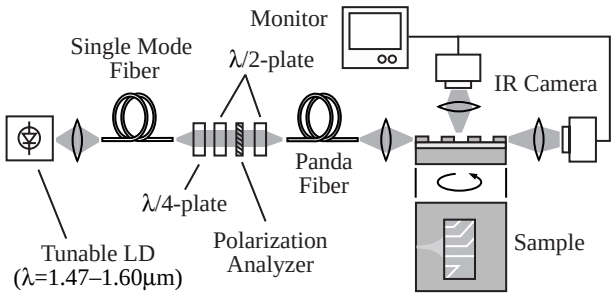

Fig. 6. Schematic of measurement setup.

tion of a $\lambda/4$ plate, $\lambda/2$ plates, polarization analyzers and polarization maintaining fibers (Panda fibers) in the light path from the laser to a piece of the cleaved wafer. We focused the laser light on the input facet of one piece. We first observed the near-field pattern (NFP) of light propagation through the slab waveguide without the photonic crystal by an infrared TV camera from the top and from the output direction. When the GaInAsP film had no cracks in the light path, we could not clearly observe the light propagation from the top due to the small light scattering in the slab. However, we confirmed the light propagation through the slab by the observation of NFP at the output facet. We also observed NFP of light through the SiO_2 lower cladding. According to the mode calculation using the interference matrix method,[16] this cladding mode suffers a large propagation loss of 430–450 dB/cm for arbitrary polarization. However, this mode may have reached the output facet due to the shortness of the cleaved piece of $\sim$1 mm in length and due to the large focused spot of the input light of $\sim 10\,\mu$m in diameter, which coupled to the thick SiO_2 layer more easily. Figure 7 shows examples of NFP around the photonic crystal pattern with illustrations explaining the NFP. We observed them from the top at $\lambda = 1.51\,\mu$m and $1.59\,\mu$m. The input light was guided through a straight channel at $\lambda = 1.51\,\mu$m. It propagates and is laterally diffracted in the slab beyond the output end of the channel. Then, it reached the deep crack formed in the GaInAsP film, and was strongly scattered to space. The light of $\lambda = 1.51\,\mu$m was well-confined in the channel, thus indicating that the lateral spreading of light at the crack was clearly suppressed compared with the case of $\lambda = 1.59\,\mu$m. Such a clear channel guiding at $\lambda = 1.51\,\mu$m cannot be expected for the SiO_2 cladding mode, since the confinement factor of this mode into the GaInAsP layer is calculated to be less than 0.3%. Thus, we thought that the light propagated in the photonic crystal waveguide. We could not evaluate the lateral mode profile in the channel because of the low spatial resolution of the used optical setup. Furthermore, we could not directly observe the profile of guided light at the output end of the channel due to the difficulty of the cleavage of the wafer. However, this relatively wide channel, as shown in Fig. 5, must have maintained several modes. Another point that should be noted is the strong scattering of guided light in the channel at $\lambda = 1.51\,\mu$m. One reason considered is the scattering at nonuniform holes beside channels, as seen in Fig. 4. This is simply a technical problem that can be improved by the optimization of the fabrication process.[15] Another possible reason is the essential scattering loss in this type of waveguide. A 3-D photonic band calculation of a photonic crystal disk was reported recently.[17] Similar 3-D calculation of guided modes

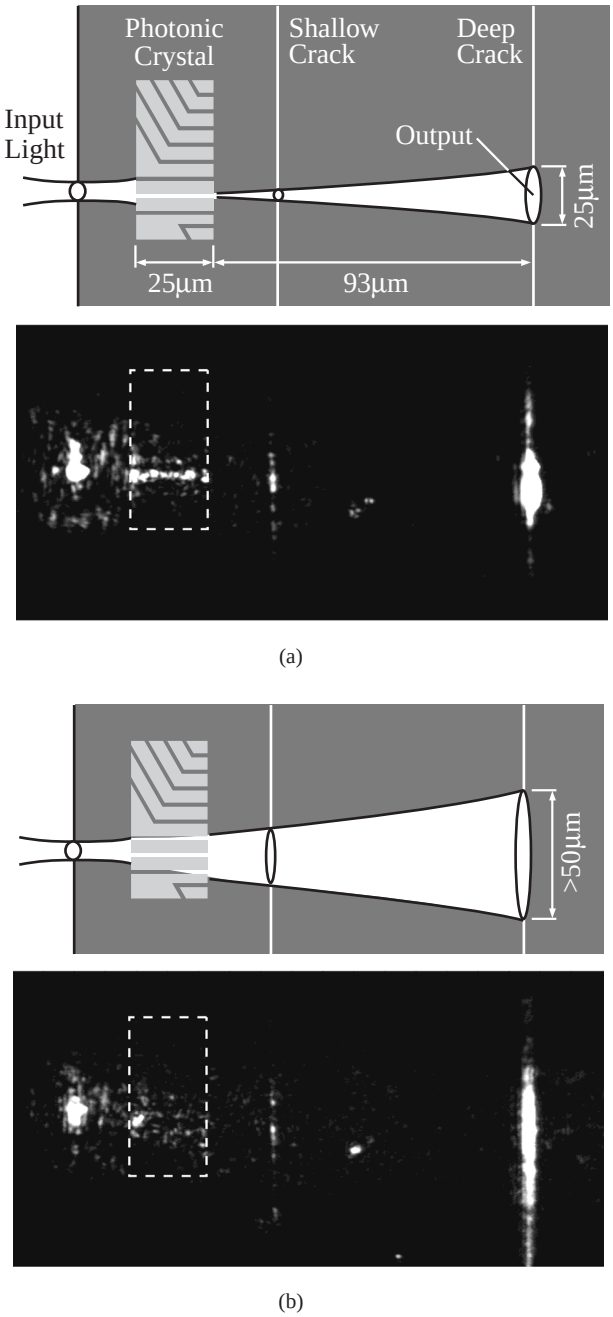

Fig. 7. NFP of light around photonic crystal pattern and explanatory illustrations. (a) and (b) are at $\lambda = 1.51\,\mu$m and $1.59\,\mu$m, respectively.

in the waveguide will be an important issue in the analysis of the experimental results.

From the different lateral spreading of light at the crack, we can specify the photonic bandgap of the crystal, as shown in Fig. 8; we measured the light intensity at the position shown in the illustration of Fig. 8 and plotted it for various wavelengths. For $\lambda \leq 1.50\,\mu$m, the intensity was almost constant, since it reached the saturation level of the TV camera. For $\lambda = 1.51$–$1.55\,\mu$m, the decay of the intensity was observed, which is thought to be caused by the PBG. The average attenuation of light at the center of the PBG was $\sim$5 dB or higher.

Figure 9 summarizes the wavelength and polarization dependence of the NFP. They were observed from the top without changing the condition of the observation. In these cases, there was a distance of $\sim 50\,\mu$m from the cleaved input facet to the photonic crystal pattern. Therefore, the light was lat-

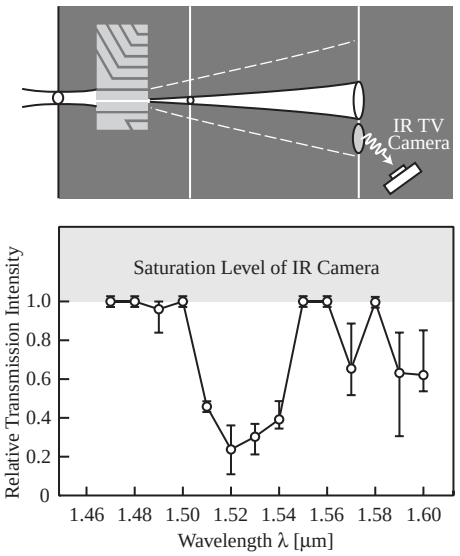

Fig. 8. Spectrum of light intensity measured at the position shown in illustration.

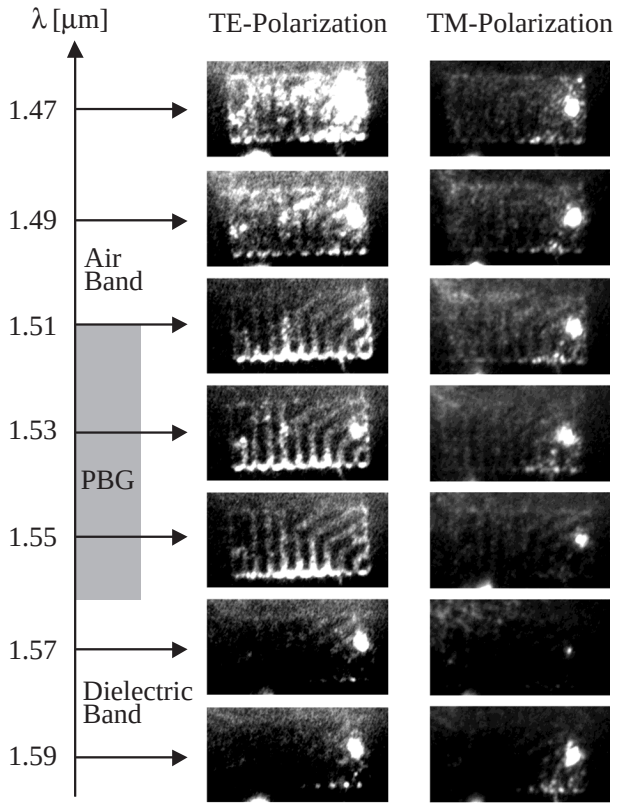

Fig. 9. Wavelength and polarization dependence of NFP observed from the top.

erally diffracted in the slab film and reached the photonic crystal pattern almost uniformly. To avoid the overlap of the guided mode and cladding mode, we rotated the input facet against the input light in the horizontal direction. Under this condition, the main axis of the guided mode was separated from that of the cladding mode due to the different refraction angle at the input facet, which was caused by different equivalent refractive indexes of these modes. Thus, the main input to the photonic crystal pattern was the guided mode. The light power that reached the pattern was thought to be almost constant for all the wavelengths and polarizations, since the intensity of the strongly scattered light seen in the right lower side of each figure in Fig. 9, which was caused by the imperfection of the slab film, was almost of the same level. At $\lambda = 1.51$–$1.56\,\mu$m, the propagation of the TE-polarized light through the channels was clearly seen from the scattered light. The propagation was still clear beyond 60° bends. We found some light spots at a crack formed very close to output ends of bent channels. From these results, we confirmed the light propagation in the bent channels, which indicated the omnidirectional reflection characteristic of the PBG in the 2-D plane. For $\lambda < 1.51\,\mu$m, strongly scattered light was observed almost uniformly from the photonic crystal pattern, and we observed that a large amount of light power passed through the pattern. This indicates the absence of the PBG. For $\lambda > 1.56\,\mu$m, the scattered light at the pattern was weak, and the light almost passed through the pattern. The lower intensity of the scattered light was partly due to the gradual decrease in the sensitivity of the TV camera used. However, the change in the sensitivity cannot be a reason for the abrupt change at $\lambda \sim 1.56\,\mu$m; it is caused by the absence of the PBG. We think that the difference of the light scattering is due to the photonic band properties. The shorter wavelengths are characterized by the photonic band called *air band*. The light passing through the crystal mainly localizes in airholes, thus the light scattering is intensified by the diffraction in the vertical direction in airholes. The longer wavelengths are characterized by the *dielectric band*; the result is opposite.

Figure 9 also shows that the light scattering was very weak for the TM polarization. This was the expected result considering that the electric field of the TM light orients similar to a p-wave against the edge of airholes. In addition, the light propagation through channels was not clear, regardless of the strength of the scattered light. This indicates the absence of PBG for this polarization. It is qualitatively consistent with the photonic band calculation shown in Fig. 3.

Compared with the calculated PBG for the TE polarization, the experimental PBG was narrow and on the side of the shorter wavelength region. This can be explained as follows. The guided mode in a thin film can be expressed by the overlap of plane waves with a broad spectrum of wave number in the vertical direction k_z. Figure 10 schematically describes the relation between the spectrum and the PBG by the 2-D calculation. The plane wave with a certain frequency range

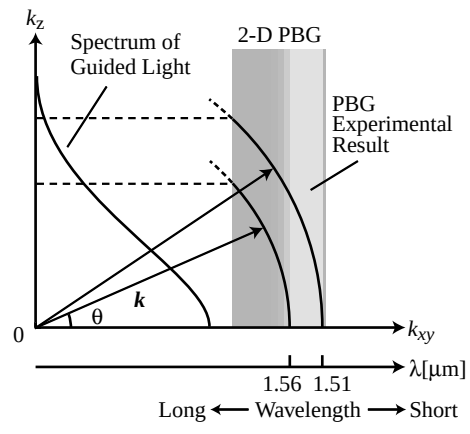

Fig. 10. Relationship between spatial frequency spectrum of guided light and 2-D PBG.

and $k_z = 0$ receives the full PBG effect. However, plane waves with the same frequency and a large k_z cannot receive the full PBG effect; the effect is negligible for the lower frequency light, viz, longer wavelength light.

5. Conclusion

We confirmed the TE PBG of the airhole photonic crystal and the light propagation in photonic crystal waveguides at $\lambda = 1.51$–$1.55\,\mu$m. These results were qualitatively consistent with theoretical ones calculated by the 2-D photonic band theory. We expect to achieve the quantitative accordance with theoretical results obtained by a 3-D calculation in a future study. The smooth light propagation with small scattering loss was observed at 60° bends. However, the essential propagation loss and bend loss in the thin slab structure should also be examined by a 3-D calculation. The waveguide demonstrated in this study was thought to be multimodal. By investigating a new design for the single-mode propagation and by lengthening waveguides, the propagation characteristics can be evaluated more clearly and quantitatively.

Acknowledgements

The authors would like to thank Professor Y. Kokubun of Yokohama National University, and Professor K. Iga and Associate Professor F. Koyama of Tokyo Institute of Technology, for their encouragement. They would also like to thank Dr. T. Miyamoto and Mr. S. Sekiguchi of Tokyo Institute of Technology, for the supply of GaInAsP/InP wafers. This work was partly supported by a Grant-in-Aid #10210203 from the Ministry of Education, Science, Sports and Culture.

1) Special Issue on Development and Applications of Materials Exhibiting Photonic Bandgaps, eds. C. M. Bowden and J. P. Dowling, J. Opt. Soc. Am. B **12** (1993) 283.
2) *Photonic Band Gaps and Localization*, ed. C. M. Soukoulis (Plenum Press, New York, 1993) NATO ASI Series B.
3) *Photonic Band Gap Materials*, ed. C. M. Soukoulis (Kluwer Academic, Dordrecht, 1996) NATO ASI Series E.
4) Microcavities and Photonic Bandgaps: Physics and Applications, eds. J. Rarity and C. Weisbuch (Kluwer Academic, Dordrecht, 1996) NATO ASI Series E .
5) J. D. Joannopoulos, R. D. Meade and J. N. Winn: *Photonic Crystals* (Princeton University Press, New Jersey, 1995).
6) T. Baba: IEEE J. Sel. Top. Quantum Electron. **3** (1997) 808.
7) Special Issue on Electromagnetic Crystal Structures, Design, Synthesis, and Applications, eds. A. Scherer, T. Doll, E. Yablonovitch, H. O. Everitt and J. A. Higgins, IEEE/OSA J. Lightwave Technol. **17** (1999) 1928.
8) A. Mekis, J. C. Chen, I. Kurand, S. Fan, P. R. Villeneuve and J. D. Joannopoulos: Phys. Rev. Lett. **77** (1996) 3787.
9) J. D. Joannopoulos, P. R. Villeneuve and S. Fan: Nature **386** (1997) 143.
10) J. Yonekura, M. Ikeda and T. Baba: IEEE/OSA J. Lightwave Technol. **17** (1999) 1500.
11) S. Y. Lin, E. Chow, V. Hietara, P. R. Valeneuve and J. D. Joannopoulos: Science **282** (1998) 274.
12) B. Temelkuran and E. Ozbay: Appl. Phys. Lett. **74** (1999) 486.
13) O. Hanaizumi, Y. Ohtera, T. Sato and S. Kawakami: Appl. Phys. Lett. **74** (1999) 777.
14) J. D. Joannopolous, P. R. Villeneuve and S. Fan: Nature **386** (1997) 143.
15) N. Fukaya, D. Ohsaki and T. Baba: Proc. Int. Workshop on Photonic and Electromagnetic Crystal Structures (2000) W4-6.
16) T. Baba, Y. Kokubun, T. Sakaki and K. Iga: IEEE/OSA J. Lightwave Technol. **6** (1988) 1490.
17) S G. Johnson, S. Fan, P R. Villeneuve, J. D. Joannopoulos and L. A. Kolodziejski: Phys. Rev. B **60** (1999) 5751.